Precision Pursuit: A Spectral Decomposition-Driven Adaptive Block Measurement Matrix for Enhanced Compressive Sensing in Imaging

Aarthi Elaveini
Department of Electronics and Communication Engineering
Faculty of Engineering and Technology, SRM Institute of Science and Technology, Ramapuram, India
aarthim@srmist.edu.in

Deepa Thangavel
Department of Electronics and Communication Engineering
Faculty of Engineering and Technology, SRM Institute of Science and Technology,Kattankulathur, India
deepat@srmist.edu.in

Abstract: *Compressive Sensing (CS) is a relatively new sophisticated technique that finds applications in various fields, and the selection of a measurement matrix influences the effectiveness of CS in image processing by identifying sparse informative pixels for sampling. The randomness in the selection of the measurement matrix results in variations in the assessment values. In this context, the Spectral Decomposition-Driven Adaptive Block Measurement Matrix (SD-DAB) method is proposed to improve the objective evaluation of images. The main aim of the proposed method is to obtain recovered images with the support of speed and quality. To accomplish this, the SD-DAB has been meticulously designed, which employs adaptive block processing, a technique that divides an image into smaller blocks and processes each block individually, adjusting the processing parameters based on the content of each block. This allows for more efficient and targeted analysis or enhancement, as the method adapts to variations in texture, brightness, or other local characteristics of the image. and the processed image matrix is analyzed with spectral decomposition. To evaluate the results, the proposed SD-DAB is contrasted with traditional methods like. The measured matrices were evaluated and compared with image quality and computational time, including the Peak Signal to Noise Ratio (PSNR), Signal to Noise Ratio (SNR), Structural Similarity Index Matrix (SSIM), and Mean Square Error (MSE). The evaluation was accomplished for distinctive sub-rates ranging from 0.1 to 0.9 and with images of varying sizes. The proposed method demonstrates superior performance at sub-rate 0.9 applied to a 512×512 sized woman with a dark hair image. It outperforms other methods with a higher PSNR of 38.49dB, SNR of 32.24dB, SSIM of 0.56, lower MSE of 9.20, and notably faster computational time of 29.61secs*.

Keywords: *Hybrid sensing matrix, sparsity, recovery algorithm, OMP, CoSaMP*.

Received February 3, 2025; accepted June 11, 2025
https://doi.org/10.34028/iajit/22/5/13

1. Introduction

The Compressive Sensing (CS) technique is a signal or image processing technique that enables the effective acquisition and reconstruction of the signal or image with fewer measurements, much smaller than the original input dimension. CS aids in image processing and compression. CS exploits the sparsity or compressibility of the images. The fundamental concept underlying CS is that several signals, such as images, can be expressed in a sparse or compressible manner within a specific basis or transform domain. CS in the context of image compression, enables the acquisition and retention of a smaller number of measurements compared to conventional approaches, while still achieving high-quality reconstruction. The process comprises three primary components sensing, sparsity representation, and reconstruction. Sensing directly samples the image pixels, and CS involves acquiring random linear pixels of the image. Samples were collected by multiplying the image with a randomized measurement matrix. The measurement of acquired sparsity is used for the reconstruction of images with fewer samples and for more efficient processing with optimization, which promotes sparsity. Typically, optimization aims to minimize the L1-norm of the transformed picture coefficients given the obtained data. Image reconstruction utilizing inverse transform on sparse pixels solves the optimization challenge. CS algorithms perform admirably in image compression, enabling high compression ratios while maintaining visual quality. Medical imaging, satellite imaging, and low-power image sensors are among the many applications of CS. It is crucial to understand that CS is simply a method of image compression, and its success is governed by the unique properties of the image and the measurement matrix utilized. Moreover, the computational complexity of the reconstruction process can pose difficulties in real-time applications. However, CS introduces new opportunities for efficient image capture, transmission, and storage. The data acquisition system follows the Nyquist-Shannon theorem, which stipulates that the sampling rate must double the bandwidth to guarantee precise information reconstruction [6]. Traditional methods are laborious

and require a large bandwidth for storing and transferring data. CS takes advantage of sparse information by reducing the sample rate [29]. Natural images contain a substantial proportion of pixel values that can be either zero or close to zero. The reconstruction of images is enabled by fewer samples and more efficient processing. Fusion of two recovery algorithms [11], such as Basis Pursuit (BP) and, Orthogonal Matching Pursuit (OMP), was used and various images were considered as input, such as test, satellite, coin, cameraman, and, MRI images of different sizes. The inference of the study shows that OMP performs with a Peak Signal to Noise Ratio (PSNR) value of 22 dB for test images, 19 dB for satellite images, and 24 dB for Magnetic Resonance Images (MRI).

Multiplication of the sparse signal with the measurement matrix is an essential step in the CS technique. It is crucial to select the measurement matrix [9] to properly select important data for transmission while retaining the necessary information for better image recovery. The Adaptive Overlap Block Compressive Sensing (Ad-OL-BCS) algorithm is applied to divided blocks of images, such as natural images and traffic signs [49]. The Poisson equation is employed in the recovery process, and the results show a better Structural Similarity Index Matrix (SSIM) of 98.14% than the traditional method, with a PSNR value of 44.28 dB. The effectiveness of PSNR shows an improved result of 20.98% and 18.98%, whereas the SSIM stands at 11.92% and 12.32%, respectively.

Parallel Compressive Sensing (PCS) for image encryption and bit-level XOR [41] enhances security and reconstruction. The image was divided into small blocks hashed by SHA-256 and quantized using bit-level XOR. The pixels are scrambled and bit XOR operations are performed on the image. The complex Hadamard measurement matrix reduces computational complexity and improves performance. The measurement matrix must adhere to both mutual coherence [8] and Restricted Isometric Property (RIP). Image reconstruction with fewer samples of sparsity is obtained by reducing the coherence [26] between the image and the column matrix. CS recovery algorithms [10, 17, 19, 23, 38] like BP, Iterative Hard Threshold (IHT), OMP, and Compressive Sampling Matching Pursuit (CoSaMP) were analyzed for better image recovery. CS finds applications [32] in diverse fields, such as medical image processing, signal processing, and communication, where the transmission of large amounts of data is achieved using fewer samples, thereby reducing storage, bandwidth, and transmission time. The approach is exemplified by techniques like few-shot segmentation [27], that address issues related to limited data availability and computational resources. Recent research has demonstrated innovative strategies such as learning what not to segment to improve focus on relevant features, leveraging base and meta-learning paradigms, and using divide-and-conquer frameworks to improve adaptability. The primary objectives of the research paper are first to design a Spectral Decomposition-Driven Adaptive Block Measurement Matrix (SD-DAB) based CS. Second, to optimize the trade-off between computational efficiency and reconstruction quality. Third to evaluate the proposed method against conventional methods at different subrates with metrics like PSNR, Signal to Noise Ratio (SNR), SSIM, Mean Square Error (MSE) and elapsed time. Inspired by these developments, the proposed SD-DAB approach integrates an adaptive measurement matrix to efficiently capture spectral and spatial characteristics, demonstrating potential applicability in both CS and other image recovery tasks. The Proposed SD-DAB divides the input image into blocks and measures the sparse pixels of the blocks adaptively and has several merits, including faster recovery time with enhanced image quality, reduced memory, and low computational complexity.

The main contribution of the proposed paper introduces spectral decomposition driven adaptive measurement matrix that dynamically adjusts based on local spectral characteristics of each block capturing the dominant frequency components resulting in textured or detailed regions and the method achieves higher fidelity and structural similarity at low subrates.

The paper is structured as follows: Section 2 presents a detailed overview of previous related studies on measurement matrices in various CS image applications section 3 introduces, the proposed SD-DAB, along with an examination of existing measurement matrices for image processing and section 4 provides a detailed tabulation and discussion of the results obtained from the proposed method compared to existing methods. Finally, section 5, concludes the paper by highlighting the significance of the different measurement matrices and the proposed SD-DAB in CS.

2. Related Works

Real-world images were validated, and data reduction was achieved by Joint Multiphase Decoding (JMD) for Block Compressive Sensing (BCS) [15]. Normalization techniques have been applied and Energy savings of 50% and 20% were obtained for block sizes of 8 and 16, respectively, for the analysis of energy consumption.

Table 1. Inference of results.

Matrix	Inference
Partial fourier matrix	Higher PSNR and higher execution time
Bernoulli Matrix (BM)	Low execution time
Hadamard Matrix (HM)	Better PSNR and fast recovery time

The performance of the CS was compared with that of traditional sampling techniques [35]. A comparison was made with a total of 3600 samples for 30 displacements with signal lengths ranging from 1 to 600 for various measurement matrices such as the Gaussian

Random Matrix (GRM), Bernoulli Random Matrix (BRM), Random Partial Fourier Matrix (RPFM), Partial Orthogonal Random Matrix (PORM), Partial Hadamard Matrices (PHM), Toeplitz Matrix (TM), and Chaotic Random Matrices (CRM). The OMP algorithm recovers the compressed signal and the result analysis is performed for the PSNR and recovery time, as shown in Table 1 above.

Xiao *et al*. [40] are proposed the design of a measurement matrix with and apple image with various matrices like GRM, BRM, PORM, PHM, and TM. The output results are analysed and finally concluded with PORMs with OMP recovery algorithm as better measurement matrix for apple image of pixel 256×256 at various sampling points M with 150,160,170,180 values with PSNR values 35.5, 36.2, 36.6 and 37.4 dB respectively. The Structurally Random Matrix (SRM) proposed by Do *et al*. [14] for a large-scale real-time CS with fast consumption that helps block processing. The SRM defines 3 steps pre-randomized, transform, and sub-sample. The complexity is reduced to a factor of $\frac{N}{4\,log\,N}$ times. Using OMP as the recovery technique, the performance analysis of the BM [47] as a sensing matrix in compressed sensing provides important new directions for efficient signal reconstruction. Various sensing matrices including partial Hadamard, random symmetric, binary, and semi-Hadamard matrices were investigated with 1024-length signal exhibiting 20 non-zero elements in the frequency domain. Recovery performance was assessed using the normalized reconstruction error metric $\frac{\|x-\hat{x}\|_2}{\|x\|_2}$. While PHM usually produce reduced reconstruction errors because of their organized character, research shows that Bernoulli matrices provide strong performance and often surpass deterministic matrices. Using full orthogonal Hadamard codes, the Bernoulli sensing matrix [25] is improved showing better performance in reconstructing binary, uniform, and Gaussian signals. Using the orthogonality of randomly selected pseudo-orthogonal columns greatly improves the columns of the sensing matrix. Perfect reconstruction was obtained in tests involving four different models with parameters I=3, B=2, p=20, β=1.25, α=0.8, and a measurement size of M=32 for a 64-dimensional signal where the SNR topped 50 dB. For image compression, the quick reconstruction of images including Boat, Barbara, and Mandrill makes use of optimized Toeplitz matrices [28] in tandem with several optimization techniques including Genetic Algorithm (GA), Particle Swarm Optimization (PSO), and Simulated Annealing (SA). BP and OMP to recover the images. A real-time framework for processing images, including Cameraman, Mandrill, and Peppers, each scaled to 128×128 pixels, is examined using TelosB nodes on the Contiki OS platform [5]. The proposed approach for image processing in Wireless Sensor Networks (WSNs) integrates a TM with OMP. Results indicate that employing Toeplitz matrices enhances image transmission and processing efficiency in resource-constrained contexts such as WSNs. Processing child and natural images of size 256×256 in a Deterministic Random Sensing Matrix (DRSM) helps to reduce storage needs [33]. This method intends to recover with OMP small coherence. PSNR is enhanced by changing the size of the sensor matrix; optimal results are found at a matrix size of 250×256 against a size of 150×256. Deep Neural Networks (DNN) are used at several sampling rates in a block-by-block approach to rebuild MRI images of the head and knee [36]. This method lets image blocks be effectively sampled and reconstructed, hence enhancing the image quality. Better reconstruction resulted in the MRI images at several sample rates-more especially, at 0.02, 0.06, 0.1, 0.3, and 0.5. A Time Division Multiple Access (TDMA) [44] method is proposed as an alternative to sparse representation for processing images of size 256×256. This approach focuses on calculating the sparsity of the measurement matrix to facilitate easier hardware implementation. The proposed chaotic measurement matrix [43] with the Chebyshev and logistic maps compresses the image into blocks for the generation of measurement values. The image peppers and cell X-ray were used for encryption, and the performance showed a better result than the ordinary measurement matrix in terms of encryption time for various compression ratios. The encryption and decryption time required for a compressive ratio of 0.25 is found to be 1.01 secs and 7.95 secs respectively. Different sampling matrices [7] such as the BRM, GRM, HM, and TM, are considered for CS applications. Sampling ratios in the range of 10-40% were considered for evaluating the matrix performance under various scenarios allowing to compare the effectiveness of each matrix in terms of the Root Mean Squared Error (RMSE) values and reconstruction time, measured in seconds. The hybrid transform-based CS [2] with the Convolutional Neural Network (CNN) technique showed a better PSNR and elapsed time for the cameraman image.

A strategy for reducing the complexity of computing for dehazing was proposed by Manoharan and Jayaseelan [22]. The convolutional capabilities of Deep Belief Neural Networks (DBN) are used for training the datasets for a shorter duration, resulting in better image quality.

A novel end-to-end deep learning framework named Adaptive Deep Convolutional Compressive Sensing Network (ADCoSNet) was designed by Shinde and Durbha [34] for adaptive 3D reconstruction of sparse Light Detection And Ranging (LiDAR) data, specifically for forests. This technique integrates Empirical Mode Decomposition (EMD) with deep convolutional CS, using the last Difficult Mode Function (IMF) as a statistical prior to effectively capturing local features. Extensive experiments conducted to test ADCoSNet showed a maximum PSNR

of 48.96 dB, which is approximately 8 dB better than reconstructions without data-dependent transforms, and a reconstruction RMSE of 7.21. Emphasizing block-based processing [3] methods, numerous CS recovery algorithms of image processing are evaluated in depth. The techniques of computational complexity, accuracy, and efficiency are examined. Segmenting images into smaller portions enables one to improve the recovery process by reducing the dimension of the problem. The results demonstrate the effectiveness of block-based CS methods, particularly in enhancing image reconstruction quality and reducing computing costs, so appropriate for real-time image processing applications. Developed for the efficient elimination of random-valued impulse noise in digital images, the region adaptive fuzzy filter [31] is a sophisticated method. Perceptual SIMilarity (PSIM) described in Equation (1) is the metric designed to combine Gradient Magnitude (GM) similarities at two scales, micro and macro structures, and colour information to predict image quality by mimicking the human visual systems [18].

$$PSIM = \frac{H_\tau}{L_\alpha \times S_\beta \times C_\theta} \tag{1}$$

where

H_τ=High distortion-based pooling, emphasizing high distortion regions.
L_α=largre scale GM similarity.
C_θ=colour information similarity.

The BCS proposed a variant of CS for images focusing on block-based processing techniques to improve the reconstruction performance of individual images and correlated images with smaller blocks and reduce computational complexity [37]. The joint reconstruction framework preserves the fine details and structures of the image and results in superior performance in terms of objective metrics. The stable signal recovery from limited and noisy measurements [12] using convex optimization techniques such as ℓ1-minimization satisfies the RIP. The method has profound implications for various applications like imaging, signal, and data compression. The signal space CoSaMP [13] is the modified version of traditional CoSaMP, designed to recover the signals which are not on standard basis but in an overcomplete dictionary. Equation (2) states D-RIP that extends RIP to signal represented in a redundant dictionary D:

$$1 - \delta_k \leq \frac{\|AD\alpha\|_2}{\|D\alpha\|^2} \leq 1 + \delta_k \tag{2}$$

where

α=sparse coefficient vector.
D=redundant dictionary.

For a signal x represented as $x=D\alpha$, the recovery error after l+1 iterations is bounded as stated in Equation (3)

$$\|x - x_{l+1}\|_2 \leq C_1\|x - x_l\|_2 + C_2\|e\|_2 \tag{3}$$

where

x_l=reconstructed signal after l iterations.
e=measurement noise.

C_1 and C_2 depend on δ_{4k} and approximation parameters $\phi 1$, $\phi 2$.

A novel block coherence [16] measures the recovery of block sparse signals providing an uncertainty relation tailored to block sparse signals thereby providing insights into the structural properties with efficient recovery. The block coherence quantifies the mutual coherence between blocks ϕ.for a measurement matrix with blocks ϕ_i and ϕ_j the block coherence is defined in Equation (4)

$$\mu_B = \max_{i=j} \frac{\|\phi_i^T \phi_j\|_2}{\|\phi_i\|_2 \|\phi_j\|_2} \tag{4}$$

where

ϕ_i and ϕ_j =Block columns of ϕ.
$\|.\|_2$=spectral norm or Euclidean norm.

Gradient Magnitude Similarity Deviation (GMSD) designed to evaluate the visual quality of images [42] which reflects edge pixel information and textures is crucial for human evaluation. The Gradient Magnitude Similarity (GMS) score is calculated for each pixel by calculating the difference between reference and distorted images that are used for computing Mean Gradient Magnitude Similarity (GMSM) with the formulas given in Equation (5).

$$GMSD = \sqrt{\frac{1}{N}\sum_{i=1}^{N}(GMS(i) - GMSM)^2} \tag{5}$$

This paper presents a novel technique called SD-DAB based Measurement Matrix, where the image is divided into smaller matrices to improve image restoration. This component enables the creation of a measuring matrix that enhances image quality and decreases recovery duration. The proposed SD-DAB maintains a high PSNR and achieves low elapsed time. To validate the efficacy of SD-DAB, a comparative analysis using the Random Gaussian Matrix (RGM), Random Bernoulli Matrix (RBM), TM, and HM measurement matrices are performed additionally, the proposed method conducts thorough and unbiased evaluations of various measurement metrics and recovery methods, resulting in a complete assessment of the performance of the proposed SD-DAB. A novel approach to CS for natural images by employing a hybrid transform-based sensing matrix [4] reports significant improvements in image quality metrics, The approach achieved a PSNR of 34.85 dB, a SSIM of 0.945, and a MSE of 5.12. Structured measurement matrices such as Toeplitz, Hadamard, and Bernoulli have been widely studied for their role in enhancing signal reconstruction performance. Simultaneously, Orthogonal Frequency

Division Multiplexing (OFDM) offers robust transmission over multipath fading channels, making it suitable for wireless image transmission. Recent studies have integrated CS with OFDM [20] to jointly address compression and reliable transmission challenges. These hybrid approaches demonstrate improved performance in terms of PSNR, SSIM, and Bit Error Rate (BER) under noisy and fading channel conditions. Conventional chaotic matrix [46] construction methods often suffer from data redundancy due to interval sampling. To address this, recent approaches use uniform chaotic sequences with binary transformation through irreversible functions, reducing correlation and storage overhead. Embedding these sequences into structured Toeplitz matrices, followed by orthogonalization via Singular Value Decomposition (SVD), further enhances matrix efficiency and reconstruction quality. Compared to traditional orthogonalization methods, SVD offers faster processing without requiring square matrices. Table 2 tabulates the details of the related work defining the pros and cons of CS in various applications. An adaptive CS method using Schur decomposition [1] to construct data-dependent sensing matrices, combined with optimized reconstruction algorithms. Their approach demonstrated superior performance, achieving a PSNR of 36.12 dB, an SSIM of 0.952, and a lower MSE of 4.26, outperforming standard CS methods and validating the effectiveness of adaptive decomposition-based sensing in natural image reconstruction.

Table 2. Summary of related work.

Ref	Method	Approach	Pros	Cons
[15]	JMD for BCS	JMD with normalization	Energy savings (50% for 8-block, 20% for 16-block)	May not scale efficiently for high-res images
[35]	Matrix comparisons	GRM, BRM, RPFM, PORM, PHM, TM, CRM	Identifies optimal matrices for different signals	High variability in performance across different matrix types
[40]	Apple image analysis	PORM with OMP on 256x256 apple image	PSNR up to 37.4 dB	Limited to specific image types/sizes
[14]	SRM	Pre-randomized, transform, sub-sample	Low complexity: N/(4logN), fast for large-scale	Limited flexibility in adaptive transforms
[47]	BM	Used in OMP with various signals	Strong performance, surpasses deterministic matrices	Sensitive to sparsity and randomness
[25]	Enhanced Bernoulli	Pseudo-orthogonal columns added	Better for binary/Uniform/Gaussian signals	Implementation complexity due to orthogonality enforcement
[28]	TM with GA/PSO/SA	Used for image compression and recovery	Optimized Toeplitz enhances quality and efficiency	Requires computationally heavy optimization algorithms
[5]	Toeplitz on WSN	128×128 images on Contiki OS with TelosB nodes	Suitable for resource-constrained environments	Constrained by hardware limitations
[33]	DRSM	Deterministic random matrix for 256×256 images	Storage-efficient, better PSNR at 250×256	Low performance at small matrix sizes
[36]	DNN for MRI	Block-by-block CS reconstruction with DNN	Effective at multiple sampling rates	Requires training data and model complexity
[44]	TDMA-based CS	Hardware-efficient matrix design	Easier hardware implementation	Less flexible for high-res images
[43]	Chaotic measurement matrix	Chebyshev and logistic maps used	Better encryption performance	High decryption time (7.95 sec at 0.25 CR)
[7]	RMSE comparison	Sampling matrices: BRM, GRM, HM, TM	Wide matrix evaluation	RMSE varies widely under different scenarios
[2]	Hybrid transform+CNN	Cameraman image recovery	Better PSNR and faster time	Model generalization not validated
[22]	DBN for dehazing	Uses deep belief nets	Better quality with less training time	May be less interpretable than traditional methods
[34]	ADCoSNet	Deep learning for 3D LiDAR recon with EMD	PSNR up to 48.96 dB, better RMSE	Tailored for LiDAR-not directly transferable to images
[3]	Block-based CS	Block segmentation to reduce complexity	Enhanced quality and real-time recovery	Block boundary artifacts possible
[31]	Region adaptive fuzzy filter	Noise removal using fuzzy logic	Effective against impulse noise	Application limited to specific noise types
[18]	PSIM Metric	Combines gradient and color features	Closer match to human vision	Complex metric computation
[37]	Joint BCS	Fine detail preservation with small blocks	Superior objective metrics	Limited to specific types of image correlation
[12]	Convex optimization	Signal recovery using $\ell 1$-minimization	Theoretically robust under RIP	Solving convex problems is slow
[13]	Signal space CoSaMP	Recovers overcomplete dictionary signals	Reduced error with theoretical bounds	Sensitive to D-RIP compliance
[16]	Block coherence	Tailored coherence measure for block sparse signals	Improved structural recovery	Complex to calculate for large blocks
[42]	GMSD	Visual quality via edge/textures	Matches human perception well	Requires reference image for comparison
[4]	Hybrid transform-based CS	Hybrid transform-based sensing matrix for natural image compression	PSNR: 34.85 dB, SSIM: 0.945, MSE: 5.12; better image quality metrics	Model generalization not validated
[20]	CS with OFDM	Integration of CS with OFDM	Improved PSNR, SSIM, and BER under noisy/fading channels	Complexity in synchronization and channel estimation
[46]	Chaotic TM+SVD	Uniform chaotic sequence, binary transformation, embedded in TM, orthogonalized via SVD	Reduced correlation, storage overhead; faster SVD processing; enhanced reconstruction	Added computational steps for binary transformation
[1]	Adaptive CS with Schur decomp.	Adaptive CS using Schur decomposition with optimized reconstruction algorithms	PSNR: 36.12 dB, SSIM: 0.952, MSE: 4.26; superior reconstruction quality	Implementation complexity for adaptive matrix construction
[21]	Iteration-free fractal +Fuzzy clustering	Combines iteration-free fractal coding with fuzzy c-means clustering on DCT coefficients	42×speedup in encoding time; only 9% PSNR reduction	Slight loss in reconstruction quality

A hybrid technique to image compression [21] uses iteration-free fractal coding and fuzzy clustering on Discrete Cosine Transform (DCT) coefficients to reduce encoding time while maintaining image quality. Traditional fractal image compression is effective at exploiting self-similarity within images, but it is computationally expensive due to extensive range-domain searches. The system suggests using mean image as the domain pool and applying One-Dimensional Discrete Cosine Transform (1D DCT) to both range and domain blocks. Fuzzy c-means clustering is used to group related domain blocks, narrowing the search to a single relevant cluster during encoding. Experimental results with standard images demonstrate that the approach delivers an average 42x speedup in encoding time while only reducing PSNR by 9%, indicating a positive trade-off between speed and reconstruction quality.

3. Methodology

The proposed SD-DAB is a novel innovative CS method designed for the optimization of the measurement matrix, thereby enhancing image recovery and efficient compression. The proposed SD-DAB is based on the principle of CS, a signal and image processing technique that acquires and reconstructs data efficiently by determining the solutions for underdetermined systems. SD-DAB outperforms traditional CS by proposing a measurement matrix that adapts the spectral properties of image blocks. The adaptiveness of SD-DAB collects essential pixel information from the image with fewer measurements by reducing the data required for accurate reconstruction. Spectral decomposition refers to the ability to analyse an image by decomposing its constituent spectral components. Decomposition identifies the features of the image more significantly, which in turn informs the adaptive block formation and process. Typically, spectral decomposition involves transforming the image data into a frequency or eigenspace, where the components are linearly uncorrelated. The adaptive block-based concept involves dividing the image into smaller blocks and measuring them separately. SD-DAB focuses on the blocks and modifies the measurement method with specific characteristics of every block, such as the sparsity or energy distribution. The localized approach provides more precise control of the measurement process by enhancing the efficiency of data acquisition and reconstruction. The measurement matrix with SD-DAB was designed to dynamically adapt to the block size using spectral analysis. The other static measurement matrices did not change based on the signal content. The adaptive measurement matrix SD-DAB was adjusted to optimize data acquisition from each block. Adaptiveness reduces redundancy and focuses on acquiring significant data, thus enabling a more efficient CS.

In practical terms, SD-DAB involves several steps: the block division divides the image into blocks of a specified size, each block indicates the spectral decomposition that identifies the key features to be preserved, and the image is divided into blocks of a specified size. Matrix adaption optimally captures essential information as a measurement matrix based on the analysis. The adapted matrix is used to measure the blocks, and these measurements are then used to reconstruct the image by utilizing sparse recovery algorithms, such as OMP or CoSaMP.

3.1. Proposed Spectral Decomposition Driven Adaptive Block (SD-DAB)

The proposed SD-DAB on the image pixels processes the image with the minimum pixel information. SD-DAB is a highly efficient method for processing pixels that contain minimal information. The effectiveness of the proposed SD-DAB was evaluated through a thorough performance comparison with established measurement matrices, including Gaussian, Bernoulli random, and Toeplitz matrices. The proposed SD-DAB was analysed using various measurement parameters to satisfy the requirements of time-constrained applications. The performance of different images of varying sizes was evaluated. Utilizing a hybrid transformation technique combining the Haar Matrix Transform and Fast Walsh Hadamard Transform (HMT+FWHT), the proposed method achieves a sparse representation of images, ensuring efficient image recovery using the OMP and CoSaMP algorithms.

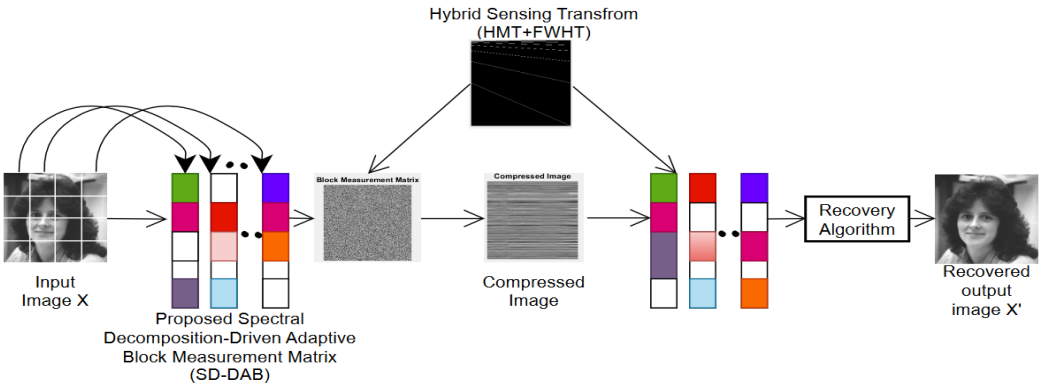

Figure 1. Proposed SD-DAB for CS.

Figure 1 presents an introductory visualization of the proposed SD-DAB, with an overview of the conceptual diagram. The block diagram provides the details of the key components and steps involved in SD-DAB, starting with the initial acquisition of the input image and its division into blocks, the application of spectral decomposition for the analyses of each block, the adaptation of the measurement matrix based on the results, and finally the reconstruction of the image in CS.

The performance of the results was compared and analysed for two different types of existing measurement matrices, random structured and deterministic matrices. In random structured matrices, such as BM and GM, the Probability Density Function (PDF) is randomly selected and obeys the RIP and mutual coherence. On the other hand, the deterministic matrix used as a measurement matrix is the TM. By evaluating the outcomes obtained from these different types of matrices using the proposed method, this study provides valuable insights into their respective performances. The proposed SD-DAB divides the image into blocks and applying spectral decomposition to analyse the sparsity and information pixels of each block, and then using the information of each block to adapt the measurement matrix accordingly.

A novel CS method proposes SD-DAB techniques that split the input matrix into smaller blocks that select only a limited number of samples from the measurement matrix. SD-DAB permits the effective processing of images by breaking down the matrix into B×B non-overlapping blocks and obtains the measurement using an appropriately sized matrix. This block-wise approach is equivalent to utilizing a whole-image measurement matrix Φ that bears a constrained structure, and the integrity of the data is maintained by simplifying the CS process. The depiction is crucial for collecting and adjusting the specific characteristics of various image segments of SD-DAB, optimizing the CS process to enhance the efficiency and image reconstruction quality. Algorithm (1) provides the algorithm of the proposed SD-DAB in detail.

Algorithm 1: The Proposed SD-DAB.

//Parameters are Initialized//
Set the block size.
Initialize the variable Φ'(0).
Set the subrate.
*Calculate N = block size * block size.*
*Calculate M = subrate * N.*
//Perform Spectral Decomposition-Driven Adaptive Block (SD-DAB)//
Decompose the input image into U, S, and V using SD-DAB.
Factorize the input image with ASV as follows:
$X \approx U * S * V'$
//The image with varying Singular values is compressed(N)//
Loop For each N in the range [5, 30, ..., 300]:
The singular value Matrix S is truncated to collect the first N Singular values.
Truncate the singular value matrix S to retain only the first N singular values.
Create a new diagonal matrix S' with the retained singular values.
Reconstruct the compressed approximation of the original image using:
$D \approx U * S' * V'$
The value of N is chosen to vary from 5 to 300 in increment of 25
//Initialize Additional Parameters//
Set Φ'(0) for the following steps.
//While N < Max Iteration//
Enter a loop that continues until N reaches the maximum allowed iterations.
Updation on the value of Φ'(t+1):
Calculate Φ'(t+1) with the formula:
$\Phi'(t+1) = \text{argmin} \; || (\Phi\psi)' H (\Phi\psi) - N ||\, N^2$
//End While: Exit the loop when N reaches the maximum allowed iterations//

3.2. Hybrid Sensing

The sensing matrix performs the transforms on the CS, and the hybrid transformation of the HMT and FWHT reduces the computational complexity. The elapsed time required for processing was minimized using the hybrid process.

3.2.1. Haar Matrix Transform (HMT)

The linear orthogonal transform used in signal processing is HMT, owing to its simplicity and efficiency in representing data, even with sudden changes, such as the image edges. HMT is well suited for image compression because of its effectiveness in capturing the hierarchical structure of spatial information, making it a more powerful tool for image processing in CS [24]. In the proposed SD-DAB, the HMT achieves sparsity using the decorrelation method on the image data, which is difficult for efficient CS. The coefficients are transformed, resulting in fewer and more significant data points required for image reconstruction.

The transformation is defined using the Haar matrix *Hn*, which is a $2^n * 2^n$ matrix used to transform a data vector, *x* of length 2^n. Matrix is constructed recursively.

For n=1, the Haar matrix $H_1$is given in Equation (6)

$$H_1 = \frac{1}{\sqrt{2}}\begin{bmatrix} 1 & 1 \\ 1 & -1 \end{bmatrix} \quad (6)$$

For any n>1, the matrix H_n can be constructed from H_{n-1} as stated in Equation (7)

$$H_n = \frac{1}{\sqrt{2}}\begin{bmatrix} H_{n-1} & H_{n-1} \\ H_{n-1}D_{n-1} & -H_{n-1}D_{n-1} \end{bmatrix} \quad (7)$$

where D_{n-1} is a diagonal matrix with diagonal elements alternating between 1 and -1, starting at 1. Equation (8) describes the Haar matrix to compute the Haar transform of vector *x* by multiplying

$$y = H_n x \quad (8)$$

where y is the transformed vector, containing both low-frequency and high-frequency components. This

process is particularly useful in image processing and data compression, where Haar transforms can efficiently reduce the data dimensionality and emphasize features. Figure 2 shows HMT applied to the image used for processing.

Figure 2. HMT on image.

Equation (9) computes inverse Haar transform using the transpose of the Haar matrix, because of its orthogonality

$$x = H_n^T y \tag{9}$$

This reverses the transformation, reconstructing the original vector from the transformed coefficients.

3.2.2. Fast Walsh Hadamard Transform (FWHT)

When paired with the HMT, the FWHM provides a reliable approach for achieving sparsity in the transformed domain. Sparsity is employed in CS to reduce the number of measurements required while maintaining critical information and boosting the speed and efficiency of the image reconstruction process.

The FWHT algorithm efficiently computes the transform without employing matrix multiplication, and the Fast Fourier Transform (FFT) improves the discrete Fourier transform. The transform of a vector x of length n can be computed recursively using the FWHT [39].

For each k from 0 to $n/2-1$ given in Equations (10) and (11).

$$y[k] = x^0[k] + x^1[k] \tag{10}$$

$$y\left[k + \frac{n}{2}\right] = x^0[k] - x^1[k] \tag{11}$$

Figure 3 gives the structure of FWHT with block size of 8.

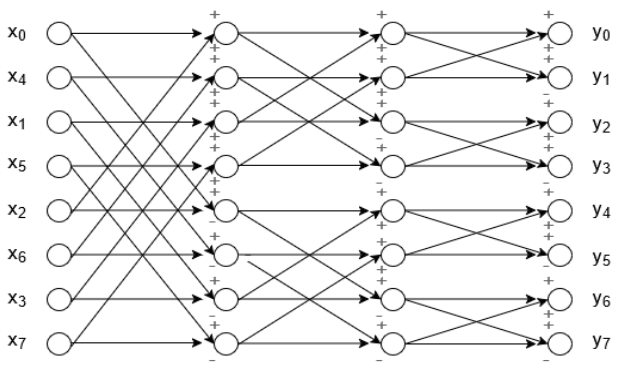

Figure 3. FWHT structure.

The inverse transform of the image performs steps similar to the transform with a scaling factor of $1/n$ to normalize the results as in Equation (12)

$$x = \frac{1}{n} H_n y \tag{12}$$

3.3. Recovery Algorithm

The CS recovery algorithm includes OMP, Greedy Algorithm (GA), BP, and CoSaMP. The proposed SD-DAB compresses the OMP or CoSaMP algorithms and outperforms with better values.

3.3.1. Orthogonal Matching Pursuit (OMP)

The greedy algorithm used for sparse image recovery is OMP, which is an integral tool in the field of CS and is given in Algorithm (2). OMP reconstructs sparse images with fewer sets of linear measurements, which are commonly required for various applications, such as image processing, image compression, and machine learning.

Algorithm 2: Orthogonal Matching Pursuit (OMP).

Input:

Initialize support set S, residual r and estimated signal x

Iterative selection

Best matching column

Compute correlations between residual and columns of Φ

$$c=\Phi^T r$$

$$j=arg\ max|c|$$

Update support set

$$S=S\cup\{j\}$$

Least Squares

$$x_S=arg\ min\|y-\Phi_S x_S\|_2$$

- *Update residual*

$$r=y-\Phi_S x_S$$

Output

3.3.2. Compressive Sampling Matching Pursuit (CoSaMP)

CoSaMP is an iterative algorithm used for reconstructing sparse signals from compressed measurements, and is applicable in fields of CS, image reconstruction, and signal processing. CoSaMP is known for its robust performance and accurate theoretical reconstruction. CoSaMP improves upon the basic greedy algorithms by refining the support of the sparse signal in a structured manner as given in Algorithm (3).

Algorithm 3: Compressive Sampling Matching Pursuit (CoSaMP).

Input:

Sensing matrix Φ*, Measurement vector y and sparsity level K*

Initialize residual r=y and estimated signal x=0

Iterative selection

Best matching column

Compute correlations between residual and columns of Φ

$$c=\Phi^T r$$

Select the top 2K indices from $|c|$

Update support set

$$S'=S\cup T$$

Least Squares

$$x_S = arg\ min\|y - \Phi_S' x_S'\|_2 \rangle\!\rangle$$

Prune approximation

K largest entries in x_S' *and update S*

Update residual

$$r = y - \Phi_S x_S$$

Output

3.4. Objective Assessment

The image was assessed using Full Reference (FR) and measured based on various parameters, including PSNR, MSE, SSIM, SNR, and computational time.

MSE is defined in Equation (13)

$$MSE = \frac{1}{mn} \sum_{i=0}^{m-1} \sum_{j=0}^{n-1} [I(i,j) - K(i,j)] \quad (13)$$

where

$I(i,j)$=input image.
$K(i,j)$=output image.

PSNR is given in Equation (14)

$$PSNR = 20 \log_{10} \left(\frac{\text{MAX}.value\ 2}{\sqrt{MSE}} \right) \quad (14)$$

Equation (15) gives the SSIM measures image quality degradation [30] caused by data compression or transmission.

$$SSIM(x,y) = \frac{(2\mu_x\mu_y + c_1)(2\sigma_x y + c_2)}{(\mu_x^2 + \mu_y^2 + c_1)(\sigma_x^2 + \sigma_y^2 + c_2)} \quad (15)$$

The PSIM [45] for grayscale images is based on comparing perceptual differences between the original and reconstructed images as given in Equation (16)

$$PSIM = \frac{H_\tau}{\left(\frac{1}{N}\sum_{i=1}^{N} I_i\right) \times S_\beta \times \sqrt{\frac{1}{N}\Sigma_{i=1}^{N}(I_i - L_\alpha)}} \quad (16)$$

The Feature Similarity Index Measure (FSIM) given in Equation (17) is a perceptual quality metric [48] used to evaluate image quality that focuses on perceptual significant features like Phase Congruency (PC) and GM.

$$FSIM = \frac{\sum_{x\in\Omega} T(x) \cdot PC_m(x)}{\sum_{x\in\Omega} PC_m(x)} \quad (17)$$

where

$T(x)$=similarity measure at pixel x, combining PC and GM similarities.
$PC_m(x)$=maximum PC value at pixel x from the reference and distorted images.
Ω=spatial domain of the image.

4. Results and Discussions

The proposed SD-DAB is assessed for efficacy with nine distinct images, including Cameraman and Peppers images, with sizes ranging from 512×512 to 96×96. The research work was conducted using an Intel Core i5 10th generation CPU laptop running MATLAB R2024b. The range of images with varying sizes and different images has been thoroughly examined using the proposed measurement matrix, which assesses the performance and effectiveness in capturing the accurate measurement of those images.

Figure 4 illustrates a comparison of the original images with the reconstructed versions using SD-DAB.

The visual assessment of the reconstructed image clearly shows the fidelity of the image, and the high quality of the reconstructed image indicates the minimum visual difference between the input image and the reconstructed image. The reconstructed images closely matched the original input image in terms of visual content and quality, confirming the effectiveness of SD-DAB in practical applications, such as in clinical diagnostics or high-precision industrial imaging. This visual demonstration also serves to validate the theoretical advantages of using an adaptive block-based approach in CS, proving its utility in real-world scenarios.

The proposed measurement matrix evaluates a diverse set of images tested under various scenarios by capturing different image characteristics, complexities, and visual contents to validate the robustness and effectiveness of the proposed measurement matrix. Figure 4-a) to (i) shows a side-by-side comparison of the original and recovered images to make judgments about the capability of the proposed method to precisely capture and reconstruct the visual information that contributes towards the advancement of image measurement techniques.

Figure 5 shows a graphical analysis of the performance of SD-DAB with various images, highlighting key metrics such as PSNR in Figure 5-a) and the MSE in Figure 5-b) The graph shows high PSNR values and low MSE values for SD-DAB compared with other measurement matrices, suggesting that SD-DAB offers superior image quality and accuracy in image reconstruction. The PSNR with a high dB value proves that the reconstructed images are similar to the original input image, and low MSE value points to minimize the error between the reconstructed and original images.

Figure 6 shows a comparison of the overall effectiveness of the proposed SD-DAB with existing measurement matrices.

The SD-DAB method results in higher PSNR and SSIM values compared with traditional methods, proving superior image quality. The high PSNR, SNR, SSIM, PSIM, and FSIM values in Figure 6-a) to (f) indicate that the reconstructed images are very close to the original images in terms of both overall intensity and structural quality.

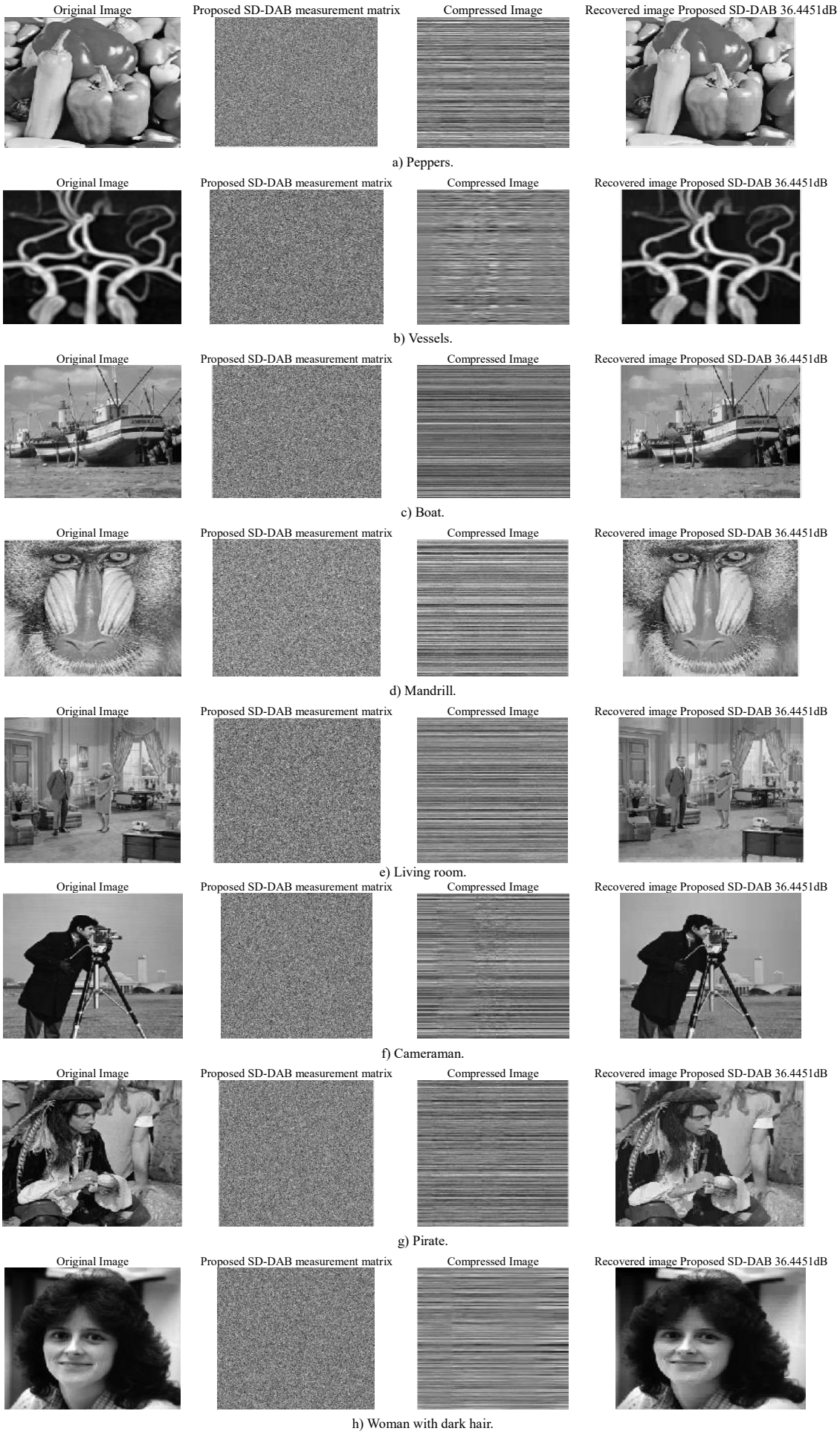

Figure 4. Original and recovered images with the proposed SD-DAB measurement matrix.

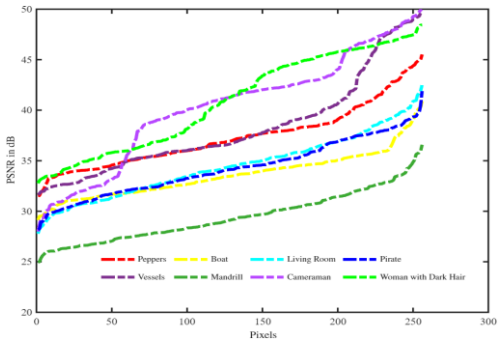

a) PSNR analysis of different images.

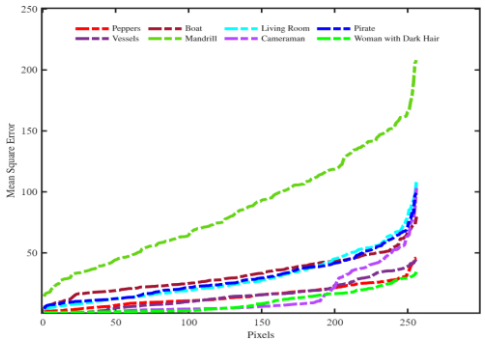

b) MSE analysis of different images.

Figure 5. PSNR and MSE comparison of proposed SD-DAB for different images.

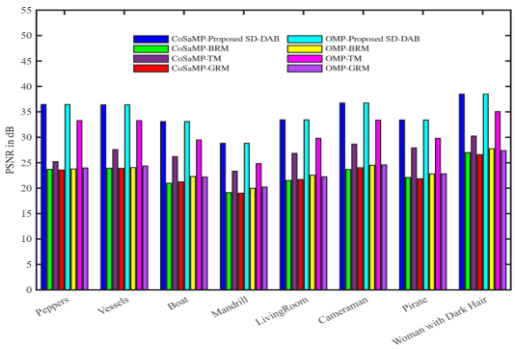

a) Average PSNR comparison with existing methods.

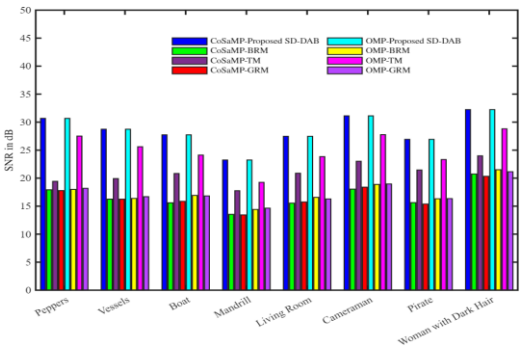

b) Average SNR comparison with existing methods.

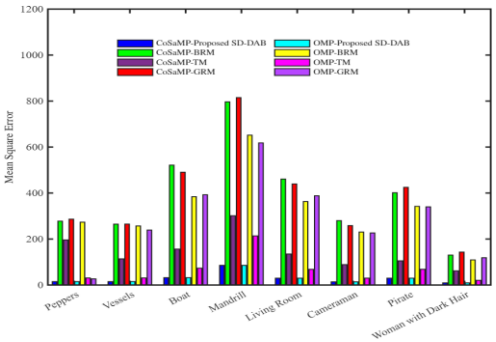

c) Average MSE comparison with existing methods.

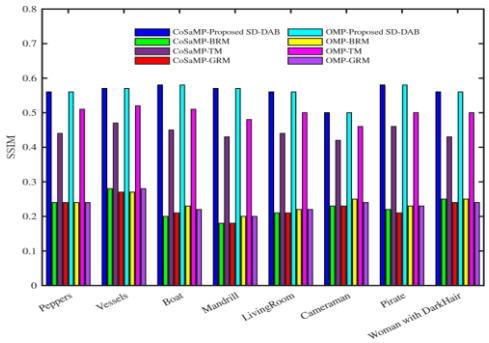

d) Average SSIM comparison with existing methods.

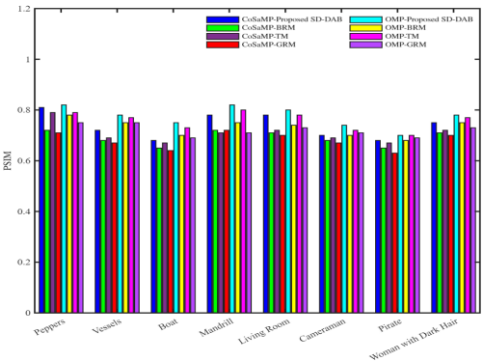

e) Average PSIM comparison with existing methods.

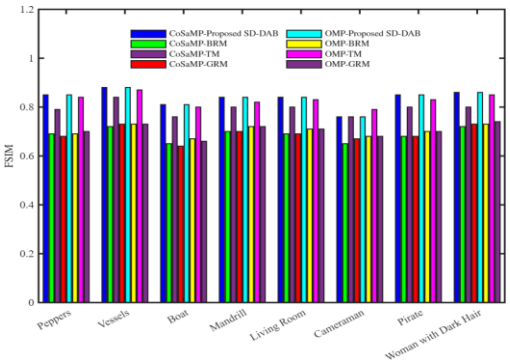

f) Average FSIM comparison with existing methods.

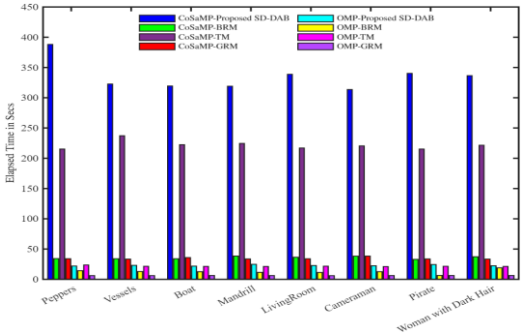

g) Average Elapsed time comparison with existing methods.

Figure 6. Average PSNR, MSE and SNR, SSIM, PSIM, FSIM, and elapsed time analysis of various images for proposed SD-DAM with the existing method.

The lower MSE values in Figure 6-c) for SD-DAB imply that it is more effective at minimizing the average squared differences between the reconstructed and original images. SD-DAB is more accurate and reliable in preserving the exact pixel values of the original image. Higher SNR values indicate that SD-DAB enhances image clarity by reducing the amount of noise in the reconstructed images. The reduced elapsed time is shown in Figure 6-e) required for image recovery of the proposed SD-DAB exhibits efficiency in the processing and reconstruction of images.

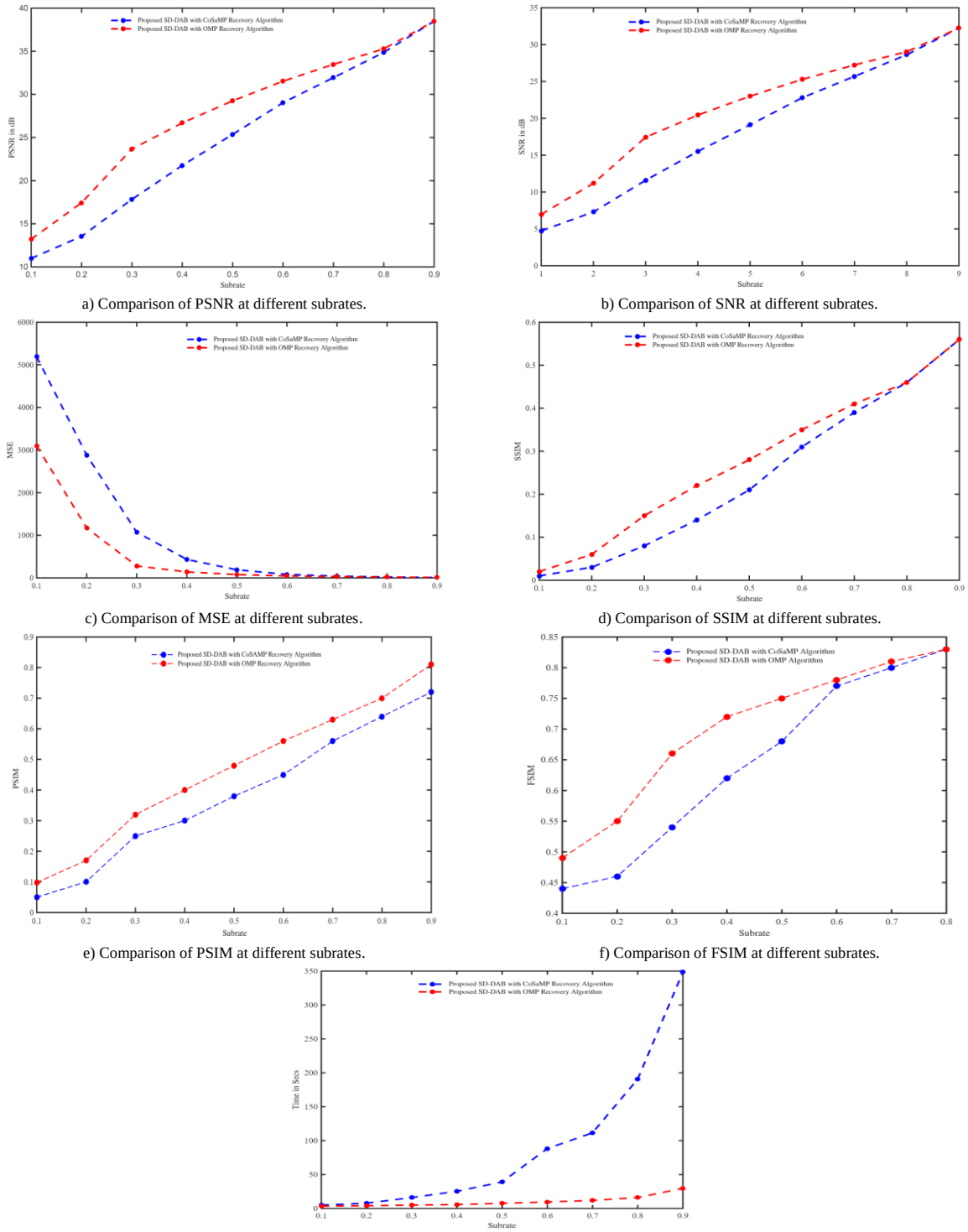

a) Comparison of PSNR at different subrates.

b) Comparison of SNR at different subrates.

c) Comparison of MSE at different subrates.

d) Comparison of SSIM at different subrates.

e) Comparison of PSIM at different subrates.

f) Comparison of FSIM at different subrates.

g) Comparison of Elapsed time at different subrates.

Figure 7. PSNR, SNR, MSE, SSIM, PSIM, FSIM and elapsed time of the proposed SD_DAB with different recovery algorithms.

Figure 7 provides a comprehensive analysis of the different reconstruction algorithms, highlighting the enhancements and limitations of the performance of the proposed SD-DAB method.

The elapsed time of the recovery algorithm on examination in Figure 7 provides advancements in system efficiency. Real-time surveillance or live medical imaging techniques require a faster recovery time with minimal compromise of image quality.

Table 3. Analysis of proposed SD-DAB at various subrate.

Recovery algorithm	Input	Subrate	0.1	0.2	0.3	0.4	0.5	0.6	0.7	0.8
CoSaMP	Woman with dark hair	PSNR	10.98	13.54	17.83	21.76	25.36	29.04	31.94	34.87
		SNR	4.73	7.29	11.59	15.51	19.11	22.79	25.69	28.62
		MSE	5.19e+03	2.88e+03	1.07e+03	433.28	189.23	81.12	41.62	21.21
		SSIM	0.01	0.03	0.08	0.14	0.21	0.31	0.39	0.46
		PSIM	0.05	0.1	0.25	0.3	0.38	0.45	0.56	0.64
		FSIM	0.44	0.46	0.54	0.62	0.68	0.77	0.80	0.83
		CR	9.85	5.02	3.33	2.51	2	1.66	1.43	1.25
		Time	4.90	7.72	16.04	25.30	39.1	88.19	111.56	190.64
	Mandrill	PSNR	14.23	15.00	16.19	17.41	18.86	19.74	21.76	26.38
		SNR	8.64	9.42	10.60	11.82	13.28	14.16	16.18	20.80
		MSE	2.46e+03	2.06e+03	1.56e+03	1.10e+03	845.35	690.33	433.20	149.58
		SSIM	0.01	0.03	0.07	0.12	0.17	0.24	0.32	0.50
		PSIM	0.08	0.15	0.29	0.39	0.5	0.56	0.62	0.71
		FSIM	0.56	0.59	0.62	0.65	0.69	0.72	0.76	0.82
		CR	9.85	5.02	3.32	2.51	2	1.66	1.43	1.2
		Time	12.79	14.23	20.42	29.90	46.84	68.83	113.06	260.27
	Living Room	PSNR	12.56	14.95	15.43	17.57	20.43	22.86	26.67	29.56
		SNR	6.60	8.99	9.48	11.61	14.47	16.90	20.71	23.60
		MSE	3.61e+03	2.08e+03	1.86e+03	1.14e+03	588.54	336.50	140.10	72.05
		SSIM	0.01	0.03	0.06	0.11	0.18	0.27	0.37	0.46
		PSIM	0.09	0.1	0.32	0.4	0.48	0.54	0.63	0.7
		FSIM	0.50	0.54	0.56	0.60	0.67	0.72	0.78	0.81
		CR	9.85	5.02	3.32	2.51	2	1.66	1.43	1.25
		Time	12.63	16.36	21.06	42.55	51.75	73.93	131.25	202.29
	Peppers	PSNR	11.21	12.82	15.06	18.05	22.26	26.20	30.13	32.73
		SNR	5.43	7.04	9.28	12.27	16.48	20.42	24.34	26.95
		MSE	4.92e+03	3.40e+03	2.03e+03	1.01e+03	386.79	155.94	63.19	34.68
		SSIM	0.01	0.03	0.07	0.12	0.21	0.31	0.40	0.47
		PSIM	0.09	0.12	0.35	0.43	0.5	0.58	0.67	0.75
		FSIM	0.43	0.45	0.49	0.56	0.66	0.74	0.78	0.82
		CR	9.85	5.02	3.33	2.51	2	1.66	1.43	1.25
		Time	13.57	14.93	22.01	30.05	47.80	72.10	114.32	196.02
OMP	Woman with dark hair	PSNR	13.21	17.43	23.67	26.69	29.25	31.53	33.48	35.28
		SNR	6.96	11.18	17.43	20.44	23.0	25.28	27.23	29.03
		MSE	3.1e+03	1.17e+03	279.04	139.33	77.34	45.77	29.2	19.29
		SSIM	0.02	0.06	0.15	0.22	0.28	0.35	0.41	0.46
		PSIM	0.1	0.17	0.32	0.4	0.48	0.56	0.63	0.7
		FSIM	0.49	0.55	0.66	0.72	0.75	0.78	0.81	0.83
		CR	9.85	5.02	3.32	2.51	2	1.66	1.43	1.25
		Time	3.43	4.05	4.93	5.73	7.48	9.53	11.8	16.06
	Mandrill	PSNR	15.27	16.97	18.21	19.40	20.67	22.17	23.54	25.22
		SNR	9.69	11.39	12.62	13.81	15.09	16.59	17.95	19.63
		MSE	1.93e+03	1.31e+03	983.02	747.27	557.10	394.57	287.92	195.63
		SSIM	0.02	0.06	0.10	0.16	0.22	0.30	0.37	0.45
		PSIM	0.09	0.13	0.34	0.43	0.52	0.62	0.68	0.74
		FSIM	0.54	0.63	0.67	0.69	0.73	0.76	0.78	0.81
		CR	9.85	5.02	3.32	2.51	2	1.66	1.43	1.25
		Time	10.79	11.81	12.37	13.32	15.12	15.85	18.35	26.61
	Living room	PSNR	15.13	16.85	18.95	21.37	23.96	26.16	28.15	30.12
		SNR	9.17	10.89	12.99	15.41	18.00	20.20	22.19	24.16
		MSE	2.0	1.34e+03	827.71	474.33	261.10	157.39	99.47	63.20
		SSIM	0.01	0.05	0.11	0.18	0.27	0.34	0.40	0.47
		PSIM	0.09	0.18	0.34	0.45	0.52	0.58	0.68	0.74
		FSIM	0.54	0.58	0.63	0.68	0.73	0.77	0.79	0.81
		CR	9.85	5.02	3.32	2.51	2	1.66	1.43	1.25
		Time	10.42	11.15	11.69	12.54	15.05	16.08	19.40	24.62
	Peppers	PSNR	12.93	15.86	18.72	23.04	25.86	28.8	30.87	32.95
		SNR	7.15	10.08	12.94	17.26	20.07	23.02	25.09	27.16
		MSE	3.31e+03	1.69e+03	872.69	323.15	168.89	85.64	53.22	33.01
		SSIM	0.02	0.06	0.12	0.20	0.29	0.36	0.41	0.47
		PSIM	0.1	0.15	0.35	0.42	0.51	0.54	0.62	0.72
		FSIM	0.46	0.52	0.58	0.68	0.73	0.76	0.80	0.81
		CR	9.85	5.02	3.32	2.51	2	1.66	1.43	1.25
		Time	10.91	11.22	12.30	13.09	17.23	18.15	18.92	24.50

Figure 7-a) to (g) depicts the variation in PSNR, MSE, SNR, SSIM, PSIM, FSIM, and recovery times between algorithms, indicating trade-offs to be addressed when selecting an algorithm. SD-DAB performs well across different recovery algorithms (high PSNR and SSIM, low MSE), it demonstrates that it is a resilient method that can be used in various computational strategies. Figure 7 provides insights that can be used to influence the selection of recovery algorithms depending on application needs. For example, if one solution performs very well in SSIM, it may be preferred for applications requiring image structural integrity, such as structural engineering and art restoration The figure not only compares the current

level of SD-DAB performance with various algorithms, but also serves as a baseline for future algorithmic strategy improvements or SD-DAB technique upgrades. The evaluation of the proposed SD-DAB algorithm is provided by extending the analysis beyond a single woman with dark hair image to additional images with varying characteristics. Mandrill, Living Room, and Peppers images pose unique challenges to test the robustness of the algorithm, under different conditions. The Mandrill image has a high texture and complicated details evaluating the algorithm's capability to preserve fine structures and handle complex frequency data. The low contrast and smooth gradient-based living room image assess the ability of the SD-DAB algorithm to recover subtle variations in intensity without artifacts. Peppers image known for its vibrant and distinct edges highlights the algorithm's performance in maintaining edge sharpness and fidelity. Comparative metrics including PSNR, SNR, MSE, PSIM, and FSIM, were computed for all four images across varying subrates in Table 3.

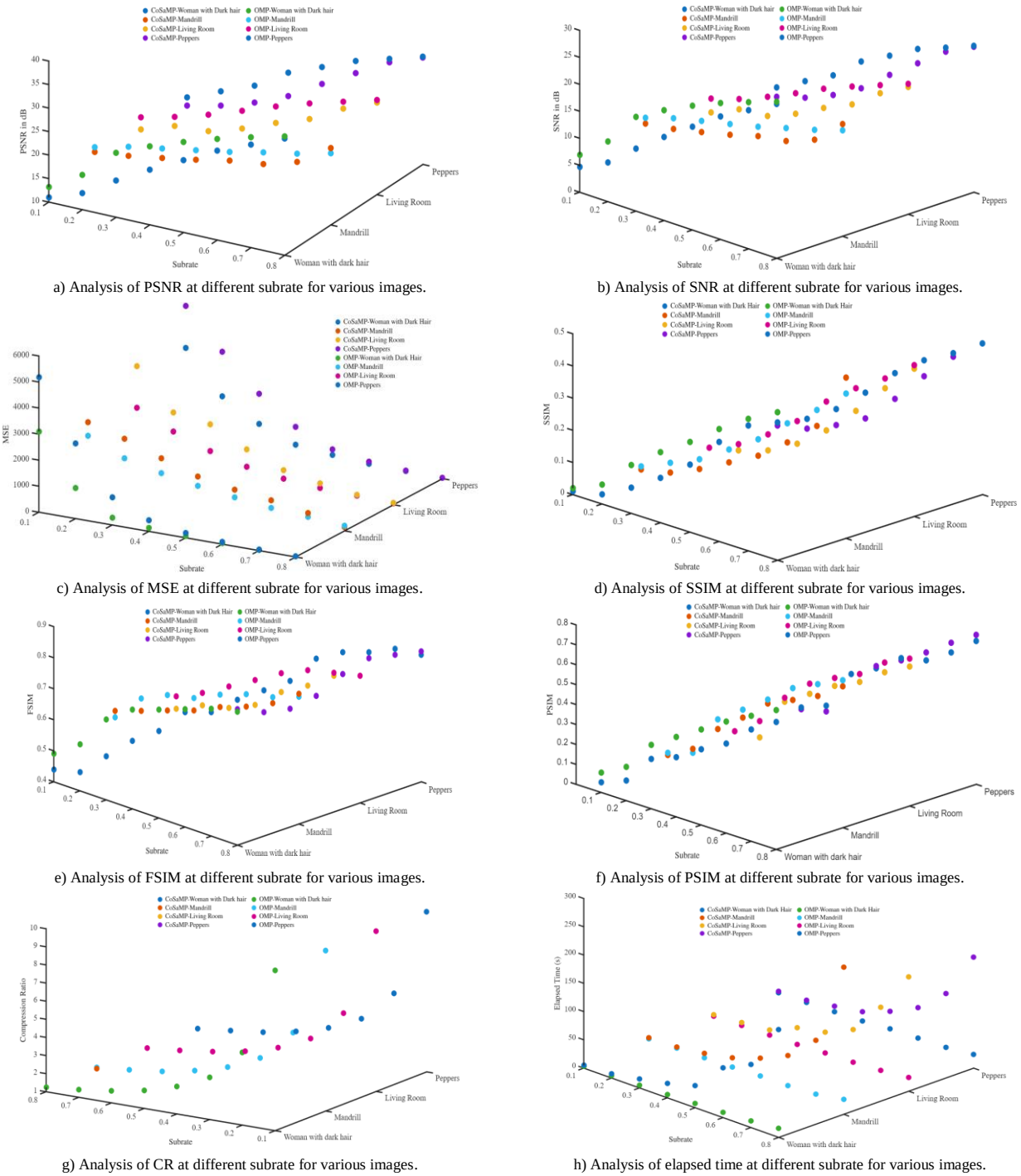

a) Analysis of PSNR at different subrate for various images.

b) Analysis of SNR at different subrate for various images.

c) Analysis of MSE at different subrate for various images.

d) Analysis of SSIM at different subrate for various images.

e) Analysis of FSIM at different subrate for various images.

f) Analysis of PSIM at different subrate for various images.

g) Analysis of CR at different subrate for various images.

h) Analysis of elapsed time at different subrate for various images.

Figure 8. Comparison of PSNR, MSE, SNR, SSIM, FSIM, PSIM, CR, and elapsed time at different subrates for the sroposed SD-DAB.

The analysis shows an increase in PSNR and a decrease in MSE values, proving that higher subrates lead to higher measurements and better reconstruction quality. The data can be used to find the minimal subrate

that achieves a satisfactory level of quality in terms of PSNR and SSIM. The performance of the recovery algorithms at various subrates indicated their robustness. The recovery algorithm with high PSNR and SSIM with various subrate ranges is suitable for versatile applications. The comparison between the elapsed time and subrates results in a trade-off between the computational speed and accuracy of the measurements. The smaller subrates result in reasonable image quality with a faster elapsed time and might be suitable for real-time appliances with a limited speed of recovery. The tabulation demonstrates that the proposed SD-DAB outperforms baseline methods, and maintain high reconstruction quality even in challenging scenarios like high texture Mandrill and low contrast living room images.

Figure 8 focuses on two different recovery algorithms CoSaMP and OMP performed on different textured images and subrates ranging from 0.1 to 0.8. various metrics like PSNR, SNR, FSIM, SSIM, PSIM, Compression Ratio, and elapsed time are considered for assessment. The analysis concludes that OMP outperforms CoSaMP for most of the metrics in terms of image quality and computational efficiency while CoSaMP provides competitive structural and feature preservation at higher rates. Both algorithms improve the reconstruction quality with increased subrates but at the cost of longer recovery time.

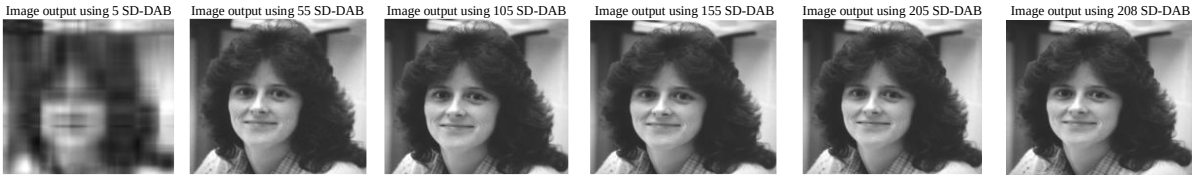

a) Output image at 5th iteration. b) Output image at 55th iteration. c) Output image at 105th iteration. d) Output image at 155th iteration. e) Output image at 205th iteration. f) Output image at 280th iteration.

Figure 9. Output image of woman with dark hair at different SD-DAB subrate values.

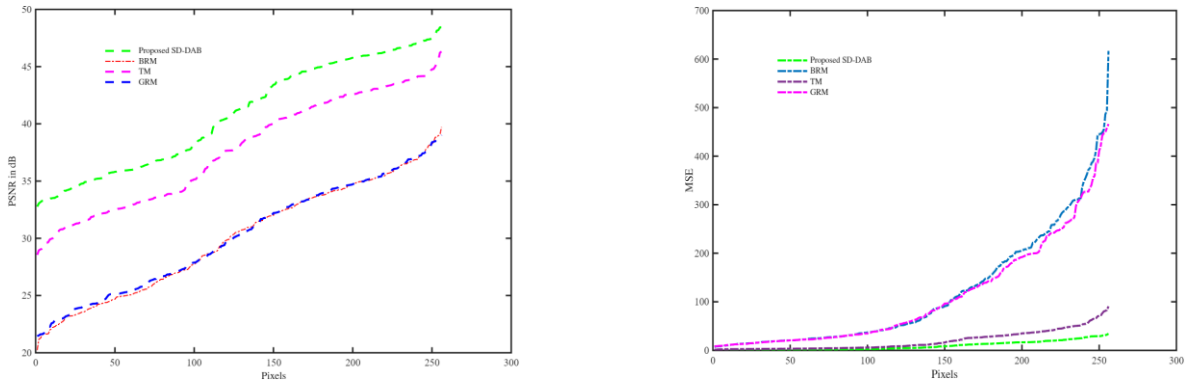

a) Overall PSNR comparison. b) Overall MSE comparison.

Figure 10. Overall comparison of PSNR and MSE of proposed SD-DAB with existing methods.

Figure 9 provides vital insights into the scalable performance of the SD-DAB method at different subrates, thus making it a useful tool for examining the practical limits and capabilities of this adaptive CS strategy. The figure shows the subrate range in which SD-DAB performs effectively. SD-DAB consistently shows better performance across a wide range of subrates compared to traditional methods, which indicates the robustness and versatility of the method in various operational contexts.

Figure 10, compares the performance of SD-DAB against traditional measurement matrices using metrics such as PSNR and MSE. Figure 10-a) shows higher PSNR values for SD-DAB compared to GRM, BRM, and TM, indicating that SD-DAB provides superior image quality. Figure 10-b) indicates the measurement of MSE for different measurement matrix with low MSE indicating better image quality. The high value of PSNR and low MSE implies the efficiency of the proposed SD-DAB in handling sparse image data more effectively than the existing methods. The superior performance of SD-DAB over traditional fixed matrices such as GRM, BRM, and TM validates the adaptive approach used in SD-DAB. Adaptation to images allows for more tailored and efficient data capture and reconstruction, affirming the benefits of using dynamic and context-sensitive measurement matrices in CS. The computational load is reduced with fewer samples, which demonstrates the effectiveness of SD-DAB in providing high-quality reconstructions.

Tables 4 provides a detailed analysis of the data compared to the performance of the proposed SD-DAB with different images and varying subrates with different recovery algorithms and values. The proposed algorithm outperforms existing methods in terms of PSNR, SSIM, and FSIM, demonstrating its effectiveness in image recovery. FSIM highlights the algorithm's ability to preserve perceptually significant features, further validating its suitability for practical applications. The PSNR and MSE values for the

proposed SD-DAB resulted in better image fidelity and accuracy in the reconstructed image. The different recovery algorithms, OMP and CoSaMP, resulted in varying effectiveness with the proposed SD-DAB. For instance, the OMP recovery algorithm results in a faster recovery time and better image quality, resulting in a trade-off between speed and accuracy. The elapsed time required for the image reconstruction tabulated in the table indicates the computational demands of the proposed SD-DAB. Real-time systems advocate for practical applications that prefer faster recovery with better image quality. The varying subrates in the SD-DAB measurement matrix show promising results in various scenarios, it is important to recognize some limitations and potential failure cases. The method's effectiveness depends on the division of block size. The proposed SD-DAB performs better for images, while it may be difficult for images with fine texture where the block size should be very small to capture the details leading to computational overhead and loss of data. The subrates below 0.1 decrease the recovery performance significantly but low subrates are desirable for reducing storage and transmission cost.

Table 4. Analysis of proposed SD-DAB with existing methods.

Recovery algorithm		**CoSaMP**				**OMP**			
Measurement matrix		**Proposed SD-DAB**	**BRM**	**TM**	**GRM**	**Proposed SD-DAB**	**BRM**	**TM**	**GRM**
Peppers 512×512	**PSNR (dB)**	36.45	23.70	25.21	23.57	36.45	23.77	33.29	23.97
	SNR (dB)	30.67	17.92	19.43	17.78	30.67	17.99	27.51	18.19
	MSE	14.74	277.69	196.04	286.17	14.74	273.13	30.46	26.53
	SSIM	0.56	0.24	0.44	0.24	0.56	0.24	0.51	0.24
	PSIM	0.81	0.72	0.79	0.71	0.82	0.78	0.79	0.75
	FSIM	0.85	0.69	0.79	0.68	0.85	0.69	0.84	0.70
	Time(secs)	388.09	34.27	215.23	34.01	21.99	14.28	23.68	6.11
Vessels 96×96	**PSNR (dB)**	36.38	23.90	27.57	23.90	36.38	24.04	33.27	24.35
	SNR (dB)	28.73	16.25	19.92	16.24	28.73	16.38	25.61	16.69
	MSE	14.64	264.64	113.67	264.95	14.94	256.78	30.64	238.91
	SSIM	0.57	0.28	0.47	0.27	0.57	0.27	0.52	0.28
	PSIM	0.72	0.68	0.69	0.67	0.78	0.75	0.77	0.75
	FSIM	0.88	0.72	0.84	0.73	0.88	0.73	0.87	0.73
	Time(secs)	322.67	33.98	237.23	33.38	23.06	12.91	21.52	6.19
Boat 512×512	**PSNR (dB)**	33.09	20.96	26.20	21.23	33.09	22.29	29.48	22.19
	SNR (dB)	27.73	15.60	20.83	15.86	27.73	16.92	24.12	16.83
	MSE	31.90	521.20	156.16	490.31	31.90	384.02	73.29	392.33
	SSIM	0.58	0.20	0.45	0.21	0.58	0.23	0.51	0.22
	PSIM	0.68	0.65	0.67	0.64	0.75	0.7	0.73	0.69
	FSIM	0.81	0.65	0.76	0.64	0.81	0.67	0.80	0.66
	Time(secs)	319.40	33.95	222.47	35.93	21.79	12.60	21.33	6.30
Mandrill 512×512	**PSNR (dB)**	28.82	19.12	23.34	19.02	28.82	19.99	24.83	20.22
	SNR (dB)	23.24	13.54	17.76	13.44	23.24	14.41	19.25	14.64
	MSE	85.35	796.37	301.23	814.83	85.35	651.54	213.49	617.86
	SSIM	0.57	0.18	0.43	0.18	0.57	0.20	0.48	0.20
	PSIM	0.78	0.72	0.71	0.72	0.82	0.75	0.8	0.71
	FSIM	0.84	0.70	0.80	0.70	0.84	0.72	0.82	0.72
	Time(secs)	319.05	38.47	224.53	33.68	24.77	11.50	21.23	6.25
Living room 512×512	**PSNR (dB)**	33.43	21.50	26.84	21.70	33.43	22.53	29.80	22.24
	SNR (dB)	27.47	15.54	20.88	15.74	27.47	16.57	23.84	16.29
	MSE	29.57	460.67	134.70	439.43	29.57	362.89	68.10	387.84
	SSIM	0.56	0.21	0.44	0.21	0.56	0.22	0.50	0.22
	PSIM	0.78	0.71	0.72	0.7	0.8	0.74	0.78	0.73
	FSIM	0.84	0.69	0.80	0.69	0.84	0.71	0.83	0.71
	Time(secs)	338.76	36.47	216.93	33.98	22.78	11.30	21.65	6.09
Cameraman 512×512	**PSNR (dB)**	36.74	23.66	28.65	24.01	36.74	24.51	33.38	24.58
	SNR (dB)	31.12	18.04	23.02	18.39	31.12	18.88	27.76	18.96
	MSE	13.77	279.73	88.76	258.24	13.77	230.31	29.84	226.35
	SSIM	0.50	0.23	0.42	0.23	0.50	0.25	0.46	0.24
	PSIM	0.7	0.68	0.69	0.67	0.74	0.7	0.72	0.71
	FSIM	0.76	0.65	0.76	0.67	0.76	0.68	0.79	0.68
	Time(secs)	313.55	38.34	220.39	38.37	22.42	12.62	21.07	6.20
Pirate 512×512	**PSNR (dB)**	33.40	22.10	27.92	21.85	33.40	22.79	29.79	22.82
	SNR (dB)	26.93	15.63	21.45	15.38	26.93	16.32	23.32	16.35
	MSE	29.70	401.03	105.08	424.60	29.70	342.19	68.29	339.81
	SSIM	0.58	0.22	0.46	0.21	0.58	0.23	0.50	0.23
	PSIM	0.68	0.65	0.67	0.63	0.7	0.68	0.7	0.69
	FSIM	0.85	0.68	0.80	0.68	0.85	0.70	0.83	0.70
	Time(secs)	340.28	32.97	215.27	33.69	24.42	6.39	21.54	6.32
Woman with dark hair 512×512	**PSNR (dB)**	38.49	27.0	30.24	26.58	38.49	27.75	35.05	27.40
	SNR (dB)	32.24	20.74	23.99	20.33	32.24	21.50	28.81	21.15
	MSE	9.20	130.15	61.49	143.05	9.20	109.09	20.31	118.43
	SSIM	0.56	0.25	0.43	0.24	0.56	0.25	0.50	0.24
	PSIM	0.75	0.71	0.72	0.7	0.78	0.75	0.77	0.73
	FSIM	0.86	0.72	0.80	0.73	0.86	0.73	0.85	0.74
	Time(secs)	336.5	37.29	221.55	33.45	22.41	18.92	21.34	6.30

5. Conclusions and Future Work

The proposed method achieves state-of-the-art results in terms of PSNR, SSIM, PSIM, and FSIM. The FSIM as a metric underscores the algorithm's capability to maintain perceptual quality and structural details, making it highly effective for real-world image recovery applications. The performance evaluation of the proposed SD-DAB with different images of varying sizes was compared with that of a traditional measurement matrix. The evaluation of the comparison results concludes that the dark hair image shows better performance in terms of PSNR values and computational time. To conduct further assessments, a woman with a dark hair image was selected, with a size of 512×512 pixels. The performance of the proposed system was analyzed using two recovery algorithms, CoSaMP and OMP, at different sub-rates. The analysis reveals that a sub rate of 0.9 produces the best results among the tested sub-rates. The image recovered using the OMP algorithm in conjunction with the proposed SD-DAB and hybrid transform achieves a PSNR value of 38.49 dB, MSE of 9.2, SNR of 32.24 dB, SSIM of 0.56, and requires a low computational time of 22.41 seconds. The proposed SD-DAB method evaluation metrics justify that the combination of the OMP algorithm and hybrid transform was effective with high fidelity in reconstructing a woman with a dark hair image. The recovered image closely resembles the original image with a high PSNR value and low MSE, whereas the high and obtained SSIM values indicate good signal quality and similarity, respectively, with less computational time. In conclusion, the proposed SD-DAB method, along with OMP as well as hybrid transformation, yields competent performance for a woman with a dark hair image with a size of 512×512 pixels with a sub-rate of 0.9. The proposed SD-DAB demonstrates effective recovery across various images with few limitations such as block size, low subrates, and computational burden. Future work will focus on addressing these limitations by enhancing the algorithm's efficiency. Furthermore, the integration of deep learning models, like CNNs or transformer-based architectures, can be used for improving reconstruction quality. Deep learning can also be used to learn optimal measurement matrices and adaptive sampling strategies, potentially replacing traditional techniques. Similarly, generative models like Generative Adversarial Networks (GANs) or diffusion models could be investigated to enhance perceptual realism and robustness in extremely low sub-rate. Finally, a lightweight deep learning framework could be designed for real-time CS recovery on edge devices with limited computational resources.

References

[1] Aarthi M. and Deepa T., "Adaptive Compressive Sensing for Natural Images Using Schur Decomposition and Optimized Reconstruction," *in Proceedings of the 4th International Conference on Sustainable Expert Systems*, Kaski, pp. 1899-1904, 2024. DOI: 10.1109/ICSES63445.2024.10763235

[2] Aarthi M. and Deepa T., "Hybrid Transform Based Compressive Sensing of Image with Better Quality Using Denoising Convolution Neural Network," *Wireless Personal Communications*, vol. 128, pp. 645-663, 2023. https://doi.org/10.1007/s11277-022-09971-w

[3] Aarthi M. and Thangavel D., "Performance Analysis of Compressive Sensing Recovery Algorithms for Image Processing Using Block Processing," *International Journal of Electrical and Computer Engineering*, vol. 12, no. 5, pp. 2088-8708, 2022. http://doi.org/10.11591/ijece.v12i5.pp5063-5072

[4] Aarthi M., Deepa T., and Bharathiraja N., "Compressive Sensing of Natural Images with Hybrid Transform based Sensing Matrix," *in Proceedings of the 3rd International Conference on Intelligent Technologies*, Hubli, pp. 1-5, 2023. DOI: 10.1109/CONIT59222.2023.10205579

[5] Aasha S., Radha S., Nirmala P., and Kishore R., "Compressive Sensing for Images Using a Variant of Toeplitz Matrix for Wireless Sensor Networks," *Journal of Real-Time Image Processing*, vol. 16, no. 5, pp. 1525-1540, 2019. https://doi.org/10.1007/s11554-016-0658-z

[6] Abo-Zahhad M., Hussein A., and Mohamed A., "Compressive Sensing Algorithms for Signal Processing Applications: A Survey," *International Journal of Communications, Network and System Sciences*, vol. 8, no. 6, pp. 197-216, 2015. DOI: 10.4236/ijcns.2015.86021

[7] Ahmed I., Khan A., Khan A., Mujahid K., and Khan N., "Efficient Measurement Matrix for Speech Compressive Sampling," *Multimedia Tools and Applications*, vol. 80, no. 13, pp. 20327-20343, 2021. https://doi.org/10.1007/s11042-021-10657-x

[8] Allen-Zhu Z., Gelashvili R., and Razenshteyn I., "Restricted Isometry Property for General p-Norms," *IEEE Transactions on Information Theory*, vol. 62, no. 10, pp. 5839-5854, 2016. DOI: 10.1109/TIT.2016.2598296

[9] Arjoune Y., Kaabouch N., El Ghazi H., and Tamtaoui A., "A Performance Comparison of Measurement Matrices in Compressive Sensing," *International Journal of Communication Systems*, vol. 31, no. 10, pp. e3576, 2018. https://doi.org/10.1002/dac.3576

[10] Arjoune Y., Kaabouch N., El Ghazi H., and Tamtaoui A., "Compressive Sensing: Performance Comparison of Sparse Recovery Algorithms," *in Proceedings of the IEEE 7th Annual Computing*

and Communication Workshop and Conference, Las Vegas, pp. 1-7, 2017. DOI: 10.1109/CCWC.2017.7868430

[11] Belgaonkar S. and Singh V., "Image Compression and Reconstruction in Compressive Sensing Paradigm," *Global Transitions Proceedings*, vol. 3, no. 1, pp. 220-224, 2022. https://doi.org/10.1016/j.gltp.2022.03.026

[12] Candes J., Romberg J., and Tao T., "Stable Signal Recovery from Incomplete and Inaccurate Measurements," Communication *Pure Applied Mathematics*, vol. 59, no. 8, pp. 1207-1223, 2006. https://doi.org/10.1002/cpa.20124

[13] Davenport M., Needell D., and Wakin M., "Signal Space CoSaMP for Sparse Recovery with Redundant Dictionaries," *IEEE Transactions on Information Theory*, vol. 59, no. 10, pp. 6820-6829, 2013. DOI: 10.1109/TIT.2013.2273491

[14] Do T., Gan L., Nguyen N., and Tran T., "Fast and Efficient Compressive Sensing Using Structurally Random Matrices," *IEEE Transactions on Signal Processing*, vol. 60, no. 1, pp. 139-154, 2012. DOI: 10.1109/TSP.2011.2170977

[15] Ebrahim M., Chia W., Adil S., and Raza K., "Block Compressive Sensing (BCS) Based Low Complexity, Energy Efficient Visual Sensor Platform with Joint Multi-Phase Decoder (JMD)," *Sensors (Basel)*, vol. 19, no. 10, pp. 1-21, 2019. https://doi.org/10.3390/s19102309

[16] Eldar Y., Kuppinger P., and Bolcskei H., "Block-Sparse Signals: Uncertainty Relations and Efficient Recovery," *IEEE Transactions on Signal Processing*, vol. 58, no. 6, pp. 3042-3054, 2010. DOI: 10.1109/TSP.2010.2044837

[17] Goklani H., Sarvaiya J., and Abdul F., "A Review on Image Reconstruction Using Compressed Sensing Algorithms: OMP, CoSaMP and NIHT," *International Journal of Image Graphics and Signal Processing*, vol. 9, no. 8, pp. 30-41, 2017. https://doi.org/10.5815/ijigsp.2017.08.04

[18] Gu K., Li L., Lu H., Min X., and Lin W., "A Fast Reliable Image Quality Predictor by Fusing Micro-and Macro-Structures," *IEEE Transactions on Industrial Electronics*, vol. 64, no. 5, pp. 3903-3912, 2017. DOI: 10.1109/TIE.2017.2652339

[19] Khosravy M., Gupta N., Patel N., and Duque C., *Compressive Sensing in Healthcare*, Elsevier Inc., 2020. https://doi.org/10.1016/B978-0-12-821247-9.00007-X

[20] Kumari A. and Kumar S., "Compressed Sensing for Image Communication with various Measurement Matrices," *Journal of Electrical Systems*, vol. 20, no. 3, pp. 4818-4828, 2024. https://journal.esrgroups.org/jes/article/view/6015

[21] Mahalingam S., Lakshapalam V., and Ekabaram S., "Image Compression Based on Iteration-Free Fractal and using fuzzy Clustering on DCT Coefficients," *The International Arab Journal of Information Technology*, vol. 14, no. 4, pp. 457-463, 2017. https://www.iajit.org/paper/4956

[22] Manoharan J. and Jayaseelan G., "Single Image Dehazing Using Deep Belief Neural Networks to Reduce Computational Complexity," *in Proceedings of the New Trends in Computational Vision and Bio-Inspired Computing*, Coimbatore, pp. 1471-1478, 2020. https://doi.org/10.1007/978-3-030-41862-5_151

[23] Marques E., Maciel N., Naviner L., Cai H., and Yang J., "A Review of Sparse Recovery Algorithms," *IEEE Access*, vol. 7, pp. 1300-1322, 2019. DOI: 10.1109/ACCESS.2018.2886471

[24] Monika R., Dhanalakshmi S., Kumar R., and Narayanamoorthi R., "Coefficient Permuted Adaptive Block Compressed Sensing for Camera Enabled Underwater Wireless Sensor Nodes," *IEEE Sensors Journal*, vol. 22, no. 1, pp. 776-784, 2022. DOI: 10.1109/JSEN.2021.3130947

[25] Nouasria H. and Et-Tolba M., "An Improved Bernoulli Sensing Matrix for Compressive Sensing," *in Proceedings of the 3rd International Symposium on Ubiquitous Networking*, Casablanca, pp. 562-571, 2017. https://link.springer.com/chapter/10.1007/978-3-319-68179-5_49

[26] Obermeier R. and Martinez-Lorenzo J., "Sensing Matrix Design via Mutual Coherence Minimization for Electromagnetic Compressive Imaging Applications," *IEEE Transactions on Computational Imaging*, vol. 3, no. 2, pp. 217-229, 2017. DOI: 10.1109/TCI.2017.2671398

[27] Pachetti E. and Colantonio S., "A Systematic Review of Few-Shot Learning in Medical Imaging," *Artificial Intelligence in Medicine*, vol. 156, pp. 102949, 2024. https://doi.org/10.1016/j.artmed.2024.102949

[28] Parkale Y. and Nalbalwar S., "Application of Compressed Sensing for Image Compression Based on Optimized Toeplitz Sensing Matrices," *EURASIP Journal on Advances in Signal Processing*, vol. 70, pp. 1-30, 2021. https://doi.org/10.1186/s13634-021-00743-5

[29] Rani M., Dhok S., and Deshmukh R., "A Systematic Review of Compressive Sensing: Concepts, Implementations and Applications," *IEEE Access*, vol. 6, pp. 4875-4894, 2018. DOI: 10.1109/ACCESS.2018.2793851

[30] Ravichandran D., Nimmatoori R., and Dhivakar A., "A Study of Medical Image Quality Assessment Based on Structural Similarity Index (SSIM)," *International Journal on Advanced Computer Theory and Engineering*, vol. 5, no. 2, pp. 31-38, 2016. http://www.irdindia.in/journal_ijacte/pdf/vol5_iss2/9.pdf

[31] Roy A., Manam L., and Laskar R., "Region

Adaptive Fuzzy Filter: An Approach for Removal of Random-Valued Impulse Noise," *IEEE Transactions on Industrial Electronics*, vol. 65, no. 9, pp. 7268-7278, 2018. DOI: 10.1109/TIE.2018.2793225

[32] Sankararajan R., Rajendran H., and Sukumaran A., *Compressive Sensing for Wireless Communication: Challenges and Opportunities*, River Publishers, 2016. DOI:10.1201/9781003337652-11

[33] Sharanabasaveshwara H. and Herur S., "Designing of Sensing Matrix for Compressive Sensing and Reconstruction," *in Proceedings of the 2nd International Conference on Advances in Electronics, Computers and Communications*, pp. 1-5, 2018. DOI: 10.1109/ICAECC.2018.8479466

[34] Shinde R. and Durbha S., "Deep Convolutional Compressed Sensing-based Adaptive 3D Reconstruction of Sparse LiDAR Data: A Case Study for Forests," *Remote Sensing*, vol. 15, no. 5, pp. 1-25, 2023. https://doi.org/10.3390/rs15051394

[35] Srinivas K., Srinivas N., Kumar P., and Pradhan G., "Performance Comparison of Measurement Matrices in Compressive Sensing," *in Proceedings of the 2nd International Conference on Advances in Computing and Data Sciences*, Dehradun, pp. 342-351, 2018. https://doi.org/10.1007/978-981-13-1810-8_34

[36] Ul Haq E., Jianjun H., Huarong X., and Li K., "Block-based Compressed Sensing of MR Images Using Multi-Rate Deep Learning Approach," *Complex and Intelligent Systems*, vol. 7, no. 5, pp. 2437-2451, 2021. https://doi.org/10.1007/s40747-021-00426-6

[37] Unde A. and Deepthi P., "Block Compressive Sensing: Individual and Joint Reconstruction of Correlated Images," *Journal of Visual Communication and Image Representation*, vol. 44, pp. 187-197, 2017. https://doi.org/10.1016/j.jvcir.2017.01.028

[38] Wahid A., Shah J., Khan A., Ahmed M., and Razali H., "Multi-Layer Basis Pursuit for Compressed Sensing MR Image Reconstruction," *IEEE Access*, vol. 8, pp. 186222-186232, 2020. DOI: 10.1109/ACCESS.2020.3028877

[39] Wang L. and Zhao S., "Fast Reconstructed and High-Quality Ghost Imaging with Fast Walsh-Hadamard Transform," *Photonics Research*, vol. 4, pp. 240-244, 2016. https://doi.org/10.1364/PRJ.4.000240

[40] Xiao Y., Gao W., Zhang G., and Zhang H., "Compressed Sensing-Based Apple Image Measurement Matrix Selection," *International Journal of Distributed Sensor Networks*, vol. 11, no. 7, pp. 901073, 2015. https://doi.org/10.1155/2015/901073

[41] Xue L., Wang Y., and Wang Z., "Secure Image Block Compressive Sensing Using Complex Hadamard Measurement Matrix and Bit-Level XOR," *IET Information Security*, vol. 16, no. 6, pp. 417-431, 2022. https://doi.org/10.1049/ise2.12067

[42] Xue W., Zhang L., Mou X., and Bovik A., "Gradient Magnitude Similarity Deviation: A Highly Efficient Perceptual Image Quality Index," *IEEE Transactions on Image Processing*, vol. 23, no. 2, pp. 684-695, 2014. DOI: 10.1109/TIP.2013.2293423

[43] Yang C., Pan P., and Ding Q., "Image Encryption Scheme Based on Mixed Chaotic Bernoulli Measurement Matrix Block Compressive Sensing," *Entropy*, vol. 24, no. 2, pp. 1-23, 2022. https://doi.org/10.3390/e24020273

[44] Yang Y., Liu H., and Hou J., "A Compressed Sensing Measurement Matrix Construction Method Based on TDMA for Wireless Sensor Networks," *Entropy*, vol. 24, no. 4, pp. 1-15, 2022. https://doi.org/10.3390/e24040493

[45] Yao J., Shen J., and Yao C., "Image Quality Assessment Based on the Perceived Structural Similarity Index of an Image," *Mathematical Biosciences and Engineering*, vol. 20, no. 5, pp. 9385-9409, 2023. DOI: 10.3934/mbe.2023412

[46] Yu H. and Zhang X., "Compressed Sensing Measurement Matrix Construction Method Based on Uniform Chaotic Sequence and Matrix Factorization," *Measurement*, vol. 242, pp. 115913, 2025. https://doi.org/10.1016/j.measurement.2024.115913

[47] Zhang G., Jiao S., Xu X., and Wang L., "Compressed Sensing and Reconstruction with Bernoulli Matrices," *in Proceedings of the IEEE International Conference on Information and Automation*, Harbin, pp. 455-460, 2010. DOI: 10.1109/ICINFA.2010.5512379

[48] Zhang L., Zhang L., Mou X., and Zhang D., "FSIM: A Feature Similarity Index for Image Quality Assessment," *IEEE Transactions on Image Processing*, vol. 20, no. 8, pp. 2378-2386, 2011. DOI: 10.1109/TIP.2011.2109730

[49] Zhao H., Zhang L., Zhang Y., and Wang Y., "Imagery Overlap Block Compressive Sensing with Convex Optimization," *IEEE Transactions on Intelligent Transportation Systems*, vol. 25, no. 7, pp. 8076-8092, 2024. DOI: 10.1109/TITS.2024.3376455

Aarthi Elaveini received her B.E. degree in Electronics and Communication Engineering from Madurai Kamaraj University, Tamil Nadu, India, and her M.E. degree in Embedded Systems Technologies from Anna University, Chennai, India, in 2004 and 2012, respectively. She is currently pursuing her Ph. D at SRM University. She is currently working as an Assistant Professor in the Department of ECE, SRM Institute of Science and Technology, Ramapuram, Chennai, India. Her research interests include Wireless Communication Systems, Image Processing, and Visible Light Communication.

Deepa Thangavel Deepa (Senior Member, IEEE) received her B.E. degree in Electronics and Communication Engineering (ECE) from Madras University, Chennai, Tamil Nadu, India, in 2004, the M.Tech degree in Communication Engineering from VIT, Vellore, Chennai, in 2006, and the Ph.D. degree, in 2015. She is currently working as an Associate Professor with the Department of ECE, SRM Institute of Science and Technology, Kattankulathur, Chennai. She has more than 45 publications in SCI/SCOPUS indexed journals and 20 proceedings in international and national conferences. She is also supervising six Ph.D. scholars and two scholars awarded with Ph.D. She is an active participant in both academic and research activities. Her research interests include Wireless Communication Systems, Signal Processing, Visible Light Communication, Multicarrier and Multiple Access Technologies, and the Internet of Things (IoT).